

Powering the Coaxial Single-Turn Seed Coil of a Magnetocumulative Generator by an Explosive-Driven Shock Wave Ferromagnetic Primary Source

Contents

1. Explosive-Driven Ferromagnetic Primary Sources	452
2. Experimental	457
3. Results and Discussion	457
3.1. Principles of a Generator Design	457
3.2. Magnetic Flux Change in Shock-Wave-Compressed Hard Ferromagnet	459
3.3. Numerical Analysis of the Seed Current in the Circuit	462
3.4. Demagnetization of Nd ₂ Fe ₁₄ B Energy-Carrying Elements Under the Transverse Shock Wave Action	462
3.5. Current Produced by the Ultracompact Ferromagnetic Primary Source	462
3.6. Seeding of Spiral Mini-MCG by Explosive-Driven Ferromagnetic Primary Source	464
4. Summary	465

Abstract

The seeding of a magnetocumulative generator (MCG) by a new type of ultracompact (25 cm³ in volume) explosive-driven source of primary power has been studied experimentally together with comprehensive computer simulation. The operation of the primary power source is based on transverse shock wave demagnetization of Nd₂Fe₁₄B high-energy hard ferromagnets. The use of the design of the shock wave ferromagnetic generator (FMG) with energy-carrying element made as a hollow Nd₂Fe₁₄B cylinder magnetized along the axis has made it possible to reduce dramatically (to 0.6 g) the mass of the high explosive (C-4) necessary for the operation of the generator with an Nd₂Fe₁₄B energy-carrying element of mass 185.7 g. The FMG is capable of producing in the coaxial seeding coil of MCG a seed current with peak amplitude exceeding four kiloamperes and full width at half maximum of several tens of microseconds. The methodology was developed for digital simulation of the seeding processes in the combined FMG/MCG system. Experimental results obtained are in a good agreement with results of digital calculations performed.

1. Explosive-Driven Ferromagnetic Primary Sources

Explosive driven pulsed power generators can be considered as the most effective compact pulsed power

sources [1–3]. One of these types of power supplies is based on the idea of the demagnetization of a closed soft ferromagnetic core with a generating coil by the transverse shock wave (shock wave propagates perpendicular to the vector of magnetic induction **B**) generated by an accelerated pellet [4,5]. Typical ultimate currents for this type of generator lie in the

range $I(t)_{\max} = 700 \div 800$ A with full width at half maximum (FWHM) of $1 \div 1.3 \mu\text{s}$ [6,7], and they are limited in the main by the low energy densities stored in soft ferromagnets and the high conductivity of these materials when shock-wave compressed [8].

The density of the electromagnetic energy stored in soft ferromagnets is lower by almost four orders of magnitude than that carried and stored (for an infinitely long time) by modern high-energy hard ferromagnetic materials based on rare-earth metal compounds [9]. In this connection, it seemed to be of importance to find an effective technique for quick initiation of the "hard ferromagnetic-to-paramagnetic" phase transition in high-energy rare-earth elements hard magnetic materials with the purpose to release, within a short time, the whole of the electromagnetic energy stored in the ferromagnetic in the form of pulses of high voltage, high current, high-power microwave radiation, etc.

The recent progress on this line [10–15] utilizes the idea of the generation of high-voltage and high-current pulses through demagnetization of an open hard ferromagnetic circuit (Fig. 1). In this case, the role of the energy-carrying and demagnetized element is played by a highly coercive ferri- or ferromagnet shaped as a body of revolution, magnetized along the axis, with a wound pulse-generating coil. It should be noted that a soft ferromagnets cannot be used as an energy-carrying elements in an open ferromagnetic circuit, since in this case the energy stored in the ferromagnets is almost zero because the residual magnetic induction B_r in such a system is approximately equal to 10^{-4} T, the coercive force H_c for soft ferromagnets is generally not over 10^2 A/m [16], and thus the energy product $BH = 10^{-8}$ J/cm³.

The feasibility of pulsed power generation through the shock wave demagnetization of an open hard ferromagnetic circuit was demonstrated in [10]. The open hard ferromagnetic circuit comprised as an energy-carrying element a solid cylinder of BaFe₁₂O₁₉ hard ferrimagnet (with energy product $BH_{\max} = 2.87 \cdot 10^{-2}$ J/cm³) magnetized along the axis. Longitudinal shock-wave compression (the shock wave propagated along the magnetization vector \mathbf{M}) of the BaFe₁₂O₁₉ induced the "hard ferrimagnetic-to-paramagnetic" phase transition that ended in almost complete demagnetization of the BaFe₁₂O₁₉. A compact explosive-driven high-voltage generators were designed [10,12] (Fig. 2) that utilized the "hard ferrimagnetic-to-paramagnetic" phase transition in the BaFe₁₂O₁₉ energy-carrying element of volume 9.85 cm³. The high-voltage generators were capable of producing a quasi-triangular high-voltage pulse with amplitude up to $U(t)_{\max} = 5450$ V and $FWHM = 0.8 \mu\text{s}$. Current generators were capable of producing a quasi-rectangular current pulse with amplitude up to $I(t)_{\max} = 157$ A and $FWHM = 54.3 \mu\text{s}$ (Fig. 3).

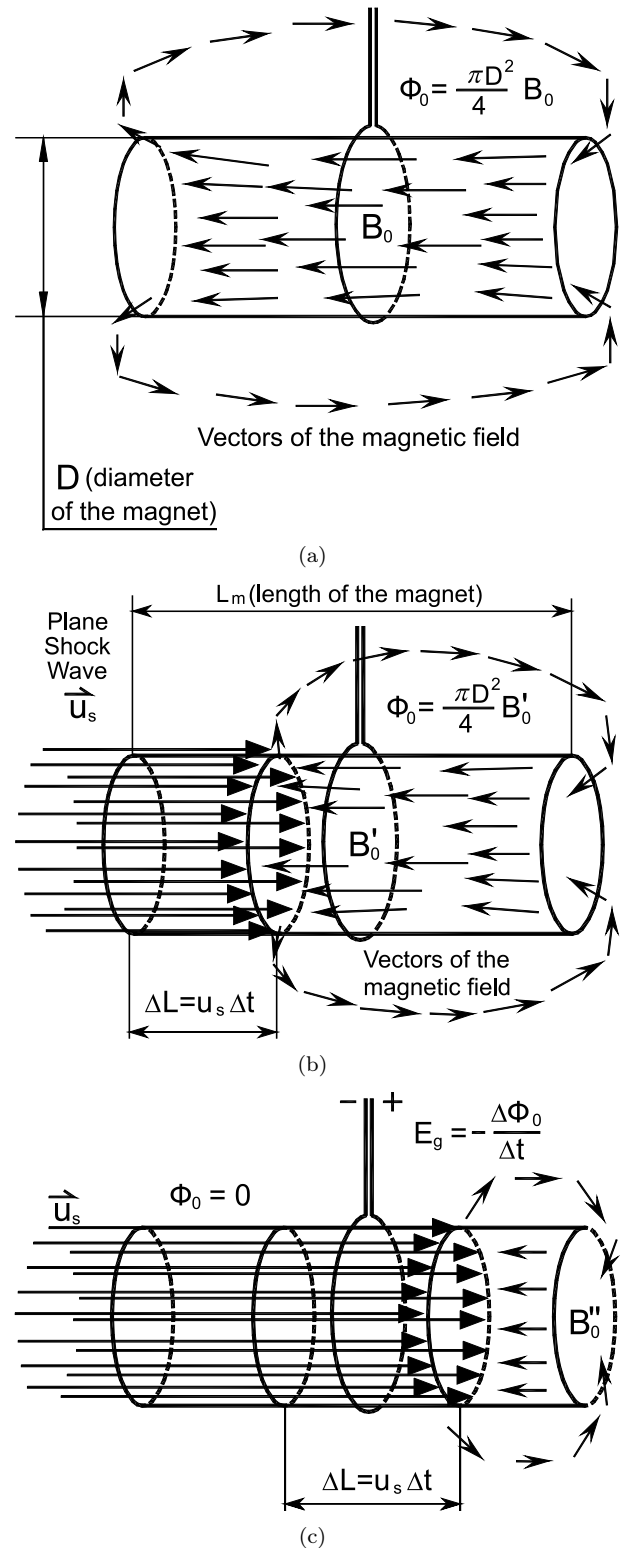


Fig. 1. Schematic diagram of the operation of the generator of primary power based on shock wave demagnetization of an open ferromagnetic circuit. (a) – initial stage of the system. (b) – shock wave travels through the magnetic cylinder and demagnetizes it. (c) – shock wave passes the winding and pulsed electromotive force is generated in the coil.

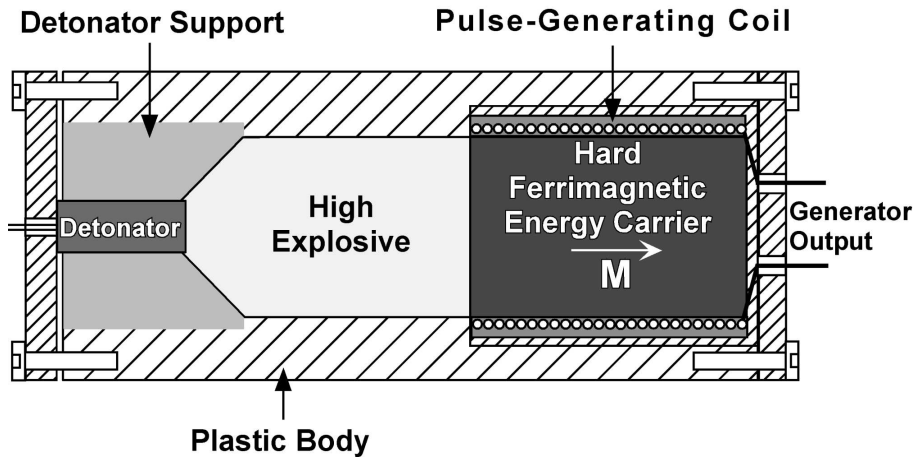


Fig. 2. Schematic diagram of the compact explosive-driven pulsed power generator based on longitudinal shock wave demagnetization of an open magnetic circuit with the $\text{BaFe}_{12}\text{O}_{19}$ hard ferrimagnetic energy-carrying element.

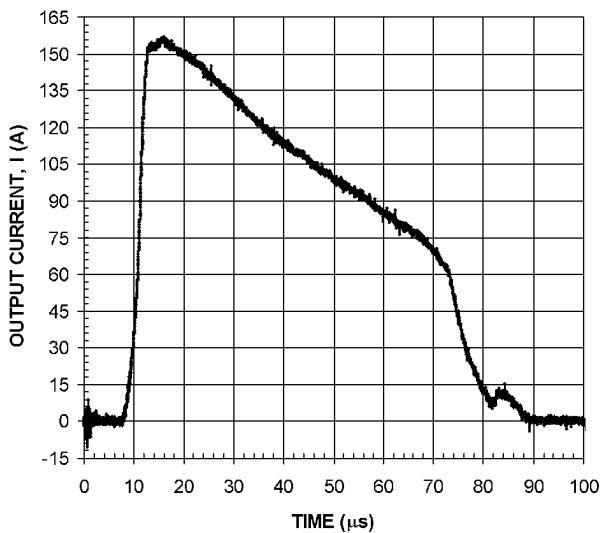


Fig. 3. Explosive operation of the compact ferromagnetic primary source containing $\text{BaFe}_{12}\text{O}_{19}$ energy-carrying element (Fig. 2). Waveforms of the current pulse obtained from the 4-turn coil wound on a $\text{BaFe}_{12}\text{O}_{19}$ cylinder (diameter $D = 2.22$ cm, length $h_0 = 2.54$ cm).

However, the density of the electromagnetic energy stored in $\text{BaFe}_{12}\text{O}_{19}$ hard ferrites is lower by an order of magnitude than that carried by modern high-energy hard ferromagnetic materials based on rare-earth metal compounds [9].

The use of high-energy rare-earth metals hard ferromagnets (with a maximum energy product $BH_{\max} = 2.79 \cdot 10^{-1} \text{ J/cm}^3$) for energy-carrying elements in explosive-driven generators based on open hard-ferromagnetic circuits was impossible until it had been revealed in [11] that a longitudinal shock-wave compression induces the "high-energy hard ferromagnetic-to-paramagnetic" phase transition in

$\text{Nd}_2\text{Fe}_{14}\text{B}$, the most high-energy ferromagnets among those commercialized by now. The explosive-driven current generator utilizing the "high-energy hard ferromagnetic-to-paramagnetic" phase transition in a $\text{Nd}_2\text{Fe}_{14}\text{B}$ energy-carrying element of volume 9.85 cm^3 (Fig. 4), described elsewhere [11], produces a quasi-triangular current pulse peaking at $I(t)_{\max} = 1000 \text{ A}$ with $FWHM = 165 \mu\text{s}$ (Fig. 5). These values are greater by more than two orders of magnitude than the respective output parameters of the generators based on the demagnetization of closed soft ferromagnetic cores [6,7].

The basic idea of the generation of high-voltage and high-current pulses through demagnetization of an open hard ferromagnetic circuit was further developed in [13], where it was established that the transverse-shock-wave compression (with the shock wave propagating across the magnetization vector \mathbf{M}) of $\text{Nd}_2\text{Fe}_{14}\text{B}$ causes the "high-energy hard ferromagnetic – to – paramagnetic" phase transition ending in almost complete demagnetization of the $\text{Nd}_2\text{Fe}_{14}\text{B}$. Based on the effect of transverse shock wave demagnetization of $\text{Nd}_2\text{Fe}_{14}\text{B}$ hard ferromagnets an ultracompact high-current pulsed generator was developed [14,15].

A major outcome of the works [13–15] is that an ultracompact explosive-driven generator (Fig. 6) has been developed which is capable of operating with a very small amount of an explosive (1 g of C-4). The energy-carrying element of the generator is an $\text{Nd}_2\text{Fe}_{14}\text{B}$ hollow cylinder magnetized along the axis (the central hole is intended for loading an explosive) (see Fig. 6). The parameters of the output current of this type of generator are almost twice those of the current generators based on longitudinal shock-wave demagnetization of $\text{Nd}_2\text{Fe}_{14}\text{B}$ [11,12].

At the same time, the overall dimensions of the ultracompact current generator [13–15] (Fig. 6) are equal, to within $0.2 \div 0.3$ cm, to those of the $\text{Nd}_2\text{Fe}_{14}\text{B}$

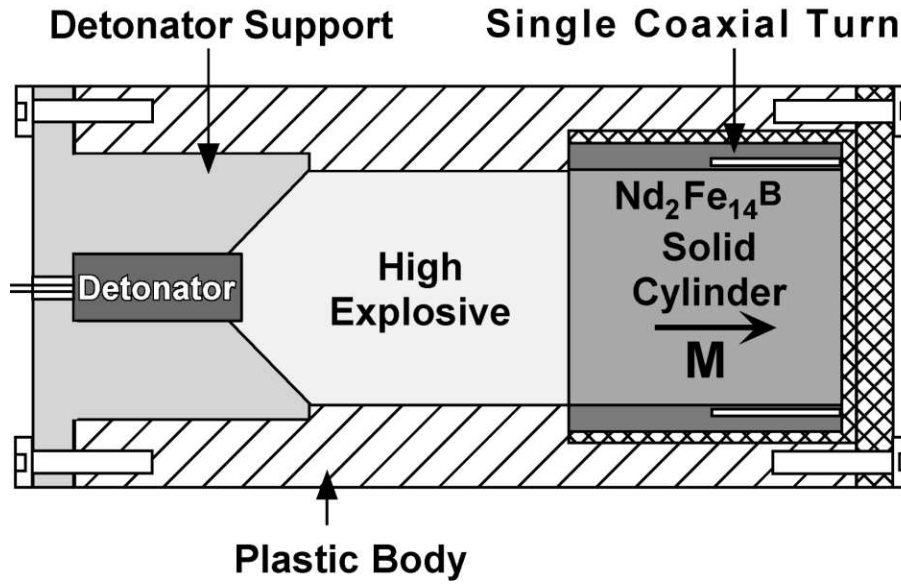


Fig. 4. Schematic diagram of the compact explosive-driven current pulsed generator based on longitudinal shock wave demagnetization of an open magnetic circuit with the $\text{Nd}_2\text{Fe}_{14}\text{B}$ hard ferromagnetic energy-carrying element.

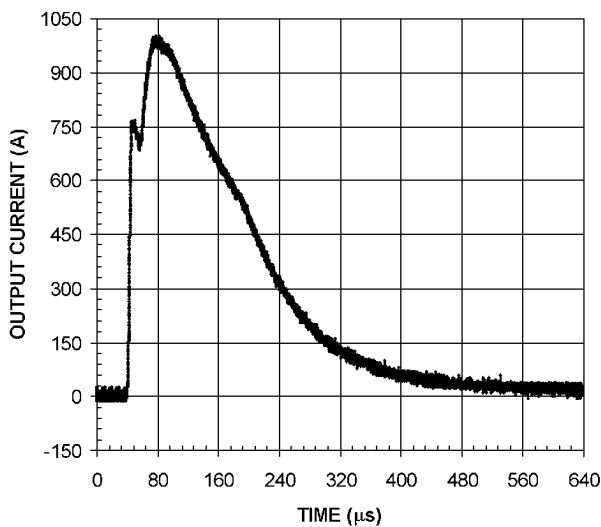


Fig. 5. Explosive-operation of the ferromagnetic primary source containing $\text{Nd}_2\text{Fe}_{14}\text{B}$ energy-carrying element (Fig. 4). Waveforms of the high-current pulse produced by the coaxial single-turn pulse-generating coil wound on an $\text{Nd}_2\text{Fe}_{14}\text{B}$ cylinder ($D = 2.22$ cm, $h_0 = 2.54$ cm).

energy-carrying element. This essentially distinguishes this type of generator from all the known explosive-driven generators [1–3,10–12] in which a considerable part of the generator volume is reserved for free movement of conductors or a flyer plate.

Another important feature of the ultracompact explosive-driven generator developed [13–15] is the short time of release of the energy stored in the $\text{Nd}_2\text{Fe}_{14}\text{B}$ energy-carrying element. It was revealed in [17], the process of pulsed release of the energy stored

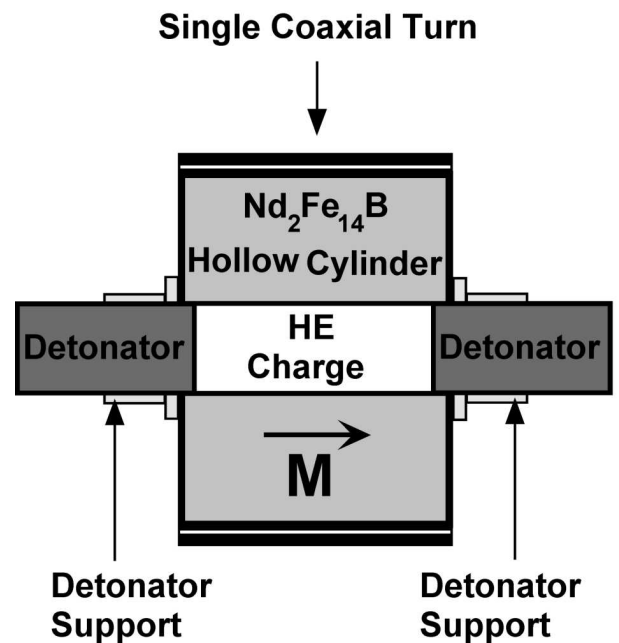


Fig. 6. Schematic diagram of the ultracompact explosive-driven primary source based on transverse shock wave demagnetization of an open magnetic circuit with the $\text{Nd}_2\text{Fe}_{14}\text{B}$ energy-carrying element.

in $\text{Nd}_2\text{Fe}_{14}\text{B}$ has a comparatively short characteristic time t which (for energy carriers with typical dimensions of $2 \div 2.5$ cm) is about $2.5 \mu\text{s}$. Thus, the energy stored in the $\text{Nd}_2\text{Fe}_{14}\text{B}$ energy-carrying element is completely released within a time $\Delta t = (1 \div 3)\tau_{\text{max}} = 2.5 \div 7.5 \mu\text{s}$.

By virtue of the foregoing, the ultracompact explosive-driven generator [13–15] based on transverse

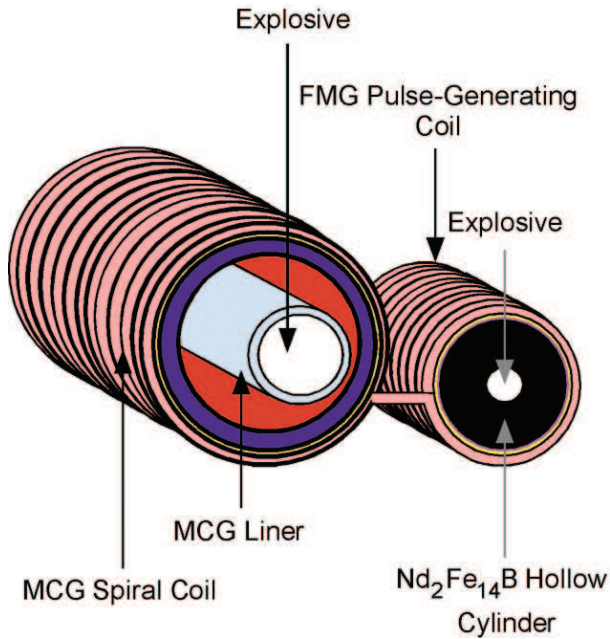


Fig. 7. Schematic diagram of an autonomous completely explosive pulsed power system utilizing ultracompact transverse shock wave ferromagnetic generator with multi-turn winding as a primary power supply and a spiral magnetocumulative generator as a pulsed power amplifier.

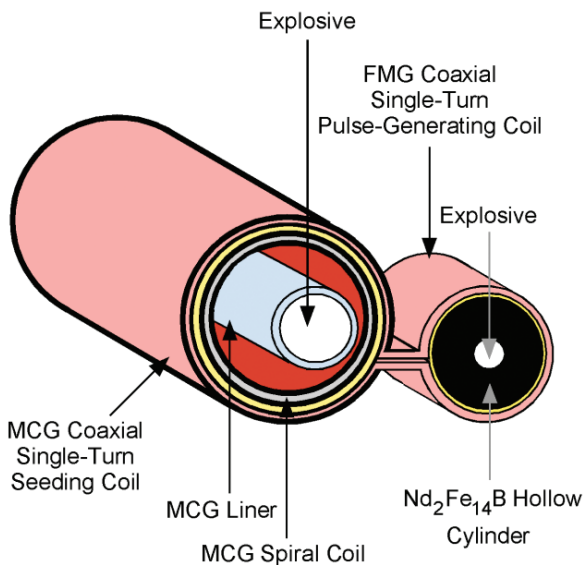


Fig. 8. Schematic diagram of an autonomous completely explosive pulsed power system utilizing ultracompact transverse shock wave ferromagnetic generator with coaxial single-turn pulse generating coil as a primary power supply and a spiral magnetocumulative generator having coaxial single-turn seeding coil as a pulsed power amplifier.

shock wave demagnetization of $\text{Nd}_2\text{Fe}_{14}\text{B}$ is a practically ideal primary energy source not only

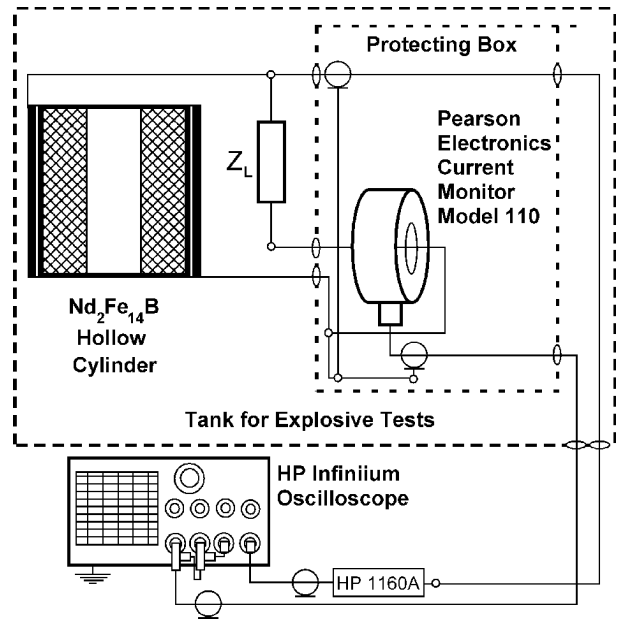


Fig. 9. Arrangement of the system for measuring seed current produced by an ultracompact FMG.

for other types of explosive-driven generator [1–3], in particular, for all types of magnetocumulative generator (MCG) that require for their operation a primary power supply (whose function can just be executed by the ultracompact current generator [13–15]), but also for conventional non-explosive high-power electronic devices, such as solid-state and e-beam generators of high-power microwaves) which demand for their operation pulsed power from tens to some thousands of kilowatts [18].

MCGs can be considered as the most effective of all existing pulsed power amplifiers [1–3]. All types of MCG need primary power to create seed magnetic field in the operating volume. The traditional method to create seed magnetic field in an MCG is a discharging of the capacitor bank into the MCG coil. It requires batteries as primary energy storage, charging circuit to charge the capacitor bank, the capacitor bank, and switches [1–3]. Replacing all these devices by an ultracompact explosive-driven generator of primary power can make pulsed power system smaller, lighter and more reliable in the operation.

An autonomous completely explosive pulsed power system being developed [19] is a combined device (Fig. 7) using the ultracompact transverse shock wave ferromagnetic generator (FMG) [13–15] as a primary power supply and a spiral MCG [1–3] as a pulsed power amplifier. The seeding system consists of two multi-turn coils connected to each other. One of this multi-turn coils wound on the $\text{Nd}_2\text{Fe}_{14}\text{B}$ energy-carrying element serves as the generating coil, the other is the seed coil of MCG (Fig. 7).

Another design of an autonomous completely explosive FMG/MCG pulsed power system is shown

in Fig. 8. The seeding system consists of two coaxial single-turn low-resistance coils which are connected by a low-inductance and low-resistance strip transmission line. One of the coaxial turns serves as the generating coil of the ultracompact FMG, while the other is the seed coil of the MCG. This design of the seeding system makes the most efficient magnetic flux transfer from the $\text{Nd}_2\text{Fe}_{14}\text{B}$ energy-carrying element to the seed volume of a magnetocumulative generator.

It should be noted that the output currents of the alternative primary power supplies based on shock-wave depolarization of piezoceramics are limited by peak values of the order of $I(t)_{\max} = 300 \div 400$ A and FWHM of $0.5 \div 2 \mu\text{s}$ [20]. These parameters of the output currents are low at least by two orders of magnitude than the tentative parameters measured for the generators based on shock-wave demagnetization of the $\text{Nd}_2\text{Fe}_{14}\text{B}$ high-energy hard ferromagnets [11–15].

In connection with the foregoing, the key problem in the development of an effective autonomous completely explosive pulsed power system is to design an effective compact explosive-driven generator of the seed current. This paper describes a study of the generation of high output currents by ultracompact generator based on transverse shock wave demagnetization of $\text{Nd}_2\text{Fe}_{14}\text{B}$ high-energy hard ferromagnets loaded on a coaxial single-turn seeding coil of an MCG.

2. Experimental

The schematic diagram of ultracompact high-current pulsed generator based on transverse shock wave demagnetization of $\text{Nd}_2\text{Fe}_{14}\text{B}$ hard ferromagnets is shown in Fig. 6. In the experiments described in this paper, the scheme of ignition with two detonators butt-jointed on both end faces of the hollow hard ferromagnetic cylinder was used. Both detonators were initiated simultaneously within ± 125 ns. The detonation velocity of C-4 is 8.04 km/s, and the dynamic pressure at the combustion front reaches 38 GPa.

The parameters of the $\text{Nd}_2\text{Fe}_{14}\text{B}$ energy-carrying elements (which were used in all experiments described in this paper) in a closed magnetic circuit are the following: residual flux density $B_r = 1.23$ T, coercive force $H_c = 8.99 \cdot 10^5$ A/m, maximum energy product $BH_{\max} = 0.279$ J/cm³; industry tolerance: $B_r \pm 5\%$, $H_c \pm 8\%$, $BH_{\max} \pm 10\%$.

The magnetic circuits of the $\text{Nd}_2\text{Fe}_{14}\text{B}$ energy-carrying elements was open, therefore, to determine the magnitude and distribution of the initial magnetic flux density, \mathbf{B}_0 , and initial magnetic flux, Φ_0 , computations using the ANSOFT Maxwell three-dimensional code [21] were carried out (the accuracy of the computations was no less than 0.03 %).

The schematic diagram of the experimental setup for measuring seed current is shown in Fig. 9. The induced current pulses were measured with a Pearson Electronics current monitor (Model 110). The Pearson Electronics current monitors were enclosed in a protective steel container specially designed for the given experiments, which was placed directly in the explosive chamber. The distance between the Pearson Electronics current monitor and the output terminals of the ultracompact generator was not over 2.5 cm. The signals from the current monitor were recorded by Hewlett-Packard Infiniium Oscilloscopes (bandwidth 500 MHz, 2 GSa/s). The output voltage pulses were attenuated with Agilent 1160A miniature passive probes (bandwidth 500 MHz, input impedance 10 MW, capacitance 9 pF) and recorded with Hewlett-Packard Infiniium Oscilloscopes. The electric circuit parameters of the system were measured with a Hewlett-Packard 4263B LCR-meter. Other experimental conditions and the equipment used corresponded to those described in [10–15,19].

3. Results and Discussion

3.1. Principles of a Generator Design

The original basic cause of generating the current by the primary sources developed in this work and in [11–15] is the appearance of electromotive force (emf) $E_g(t)$ in the pulse-generating coil due to decreasing initial magnetic flux in $\text{Nd}_2\text{Fe}_{14}\text{B}$ magnetic flux carrier under the shock wave action in accordance with Faraday's law

$$E_g(t) = -\frac{d\Phi(t)}{dt}, \quad (1)$$

where dt is the time in which the change in the magnetic flux $d\Phi(t)$ has taken place.

The current produced is a Faraday-Lentz current whose magnitude and direction are self-setting so that the magnetic flux induced by the current, $d\Phi_{\text{current}}$, compensate at the most the decreasing (due to the demagnetization) original magnetic flux, $d\Phi_{\text{NdFeB}}$, of the $\text{Nd}_2\text{Fe}_{14}\text{B}$ hard ferromagnets. Since the characteristic time τ for a decrease in original magnetic flux, Φ_{NdFeB} , determined by the basic physical processes occurring in a shock-wave compressed $\text{Nd}_2\text{Fe}_{14}\text{B}$ [17] is an essential constant for the given type of $\text{Nd}_2\text{Fe}_{14}\text{B}$ energy-carrying element, the dominant factors that limit the highest achievable current in a load are the parameters of the electric circuit carrying the current produced by the generator.

The electric circuit (Fig. 10a) that carries the seed current consists of a current-generating system (with an absolute impedance Z_G) and a load (with an absolute impedance Z_L). The load includes a current transmission line and a coaxial single-turn

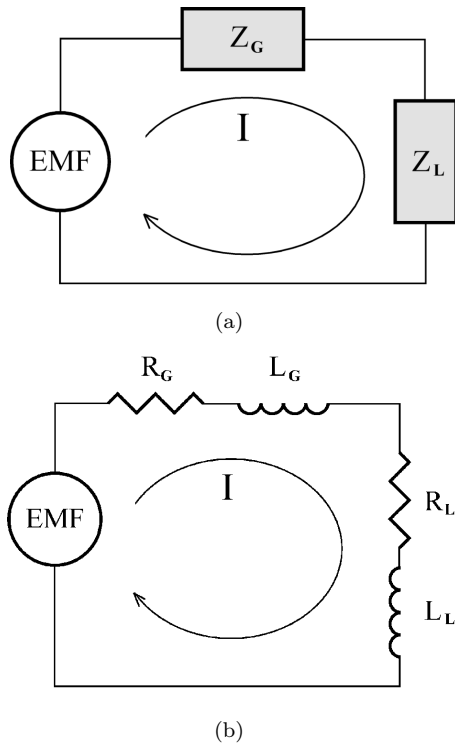


Fig. 10. Equivalent circuits of the explosive-driven transverse shock wave FMG with the MCG seeding coil served as a load (see the text).

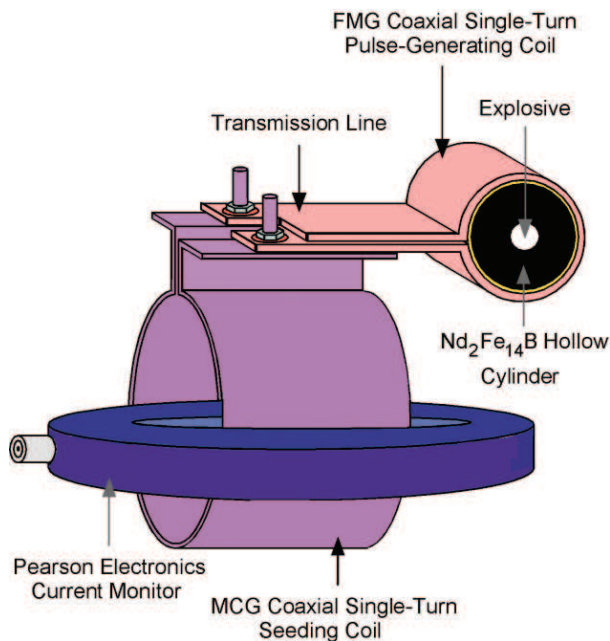
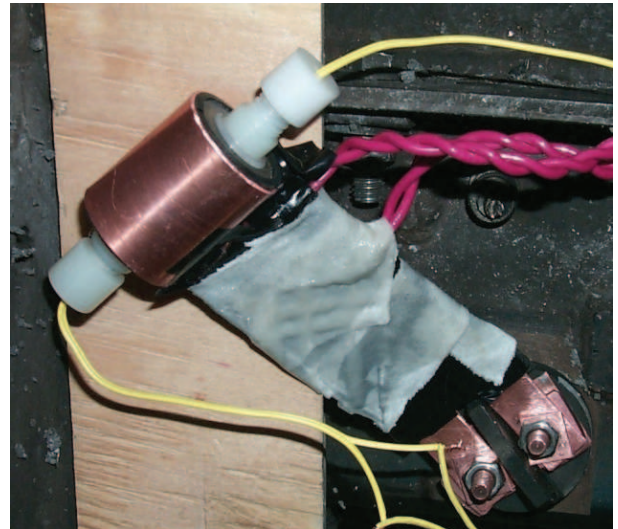


Fig. 11. Schematic diagram of the system for the seed current generating and measuring. The system contains explosive-driven ultracompact FMG as a seed source, strip transmission line, coaxial single-turn seeding coil of an MCG and commercial current monitor (Pearson Electronics, Model 110).



(a)



(b)

Fig. 12. The ultracompact FMG having Nd2Fe14B energy-carrying element ($O.D. = 5.08$ cm, $I.D. = 0.76$ cm and $h_0 = 1.27$ cm) before (a) and after (b) the high-current generation.

coil (creating the initial magnetic field in the helix of a magnetocumulative generator). Since both the generating unit and the load are inductance coils, the equivalent circuit of the whole system involves the inductance L_G and resistance R_G of the generating unit and the inductance L_L and resistance R_L of the load, connected in series (Fig. 10b). Analysis of this circuit [5,22] has shown that the maximum generated current $I_{max}(t)$ is inversely proportional to the sum of the resistive components of the circuit, $I_{max} \sim 1/(R_G + R_L)$, and the current rise rate $dI(t)/dt$ is

inversely proportional to the sum of the inductive components of the circuit, $dI(t)/dt \sim 1/(L_G + L_L)$.

Based on these requirements, the general design of the generators involved a hollow $\text{Nd}_2\text{Fe}_{14}\text{B}$ cylinder, magnetized along the axis, that was mounted in a pulse-generating system made of a one-piece copper strip of thickness 0.1 cm (with the strip width equal to the height of the $\text{Nd}_2\text{Fe}_{14}\text{B}$ cylinder) encircling the $\text{Nd}_2\text{Fe}_{14}\text{B}$ energy-carrying element with a coaxial turn and adjoining the lateral surface of the cylinder through insulating layer with the thickness of 0.16 cm (Fig. 6). The coaxial turn of the pulse-generating system went into two parallel current strips (comprising a low-inductance, low-resistance strip transmission line) spaced as closely as possible. This design made it possible to reduce at the most the inductance L_G and resistance R_G (and, hence, the absolute impedance Z_G) of the pulse-generating system.

The schematic diagram of the pulse generating system including MCG seeding coil served as a load of the FMG is shown in Fig. 11. The strip transmission line was connected by copper clumping bolt joints to the input terminals of the coaxial copper single-turn MCG seeding coil passed through a Pearson Electronics current monitor. The current flowing through this single coaxial turn (which is measured by a commercial current probe) is just the sought-for seed current.

Photographs of a typical ultracompact FMG based on transverse shock wave demagnetization of $\text{Nd}_2\text{Fe}_{14}\text{B}$, connected to the output terminals of a seed coaxial copper turn passed through a Pearson Electronics current monitor, taken before and after the test are shown in Fig. 12.

3.2. Magnetic Flux Change in Shock-Wave-Compressed Hard Ferromagnet

The change of magnetic flux in energy-carrying element is taking place as a result of "hard ferromagnetic-to-paramagnetic" phase transition in $\text{Nd}_2\text{Fe}_{14}\text{B}$ due to the shock-wave compression [11–15]. In accordance with Faraday's law Eq. (1) the change of magnetic flux $d\Phi(t)$ during time dt causes the electromotive force $E_g(t)$ in a coil wound.

As it was shown in [11,13], the single-turn diagnostic coils (made of thin copper wire) wound on the $\text{Nd}_2\text{Fe}_{14}\text{B}$ hollow cylinder and placed in different positions along the cylinder axis (z coordinate) generate electromotive force $E_g(z, t)$ of different amplitude and pulse shape. Since the ultracompact FMGs investigated in this work had single coaxial turn pulse-generating coil with the width h the $E_g(t)$ measured in the experiments is the integral

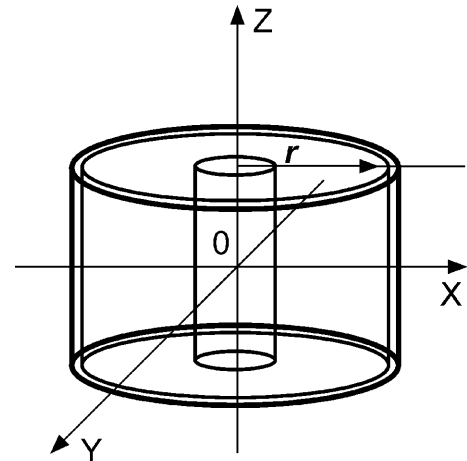


Fig. 13. The position of a coaxial single-turn coil containing $\text{Nd}_2\text{Fe}_{14}\text{B}$ hollow cylinder relatively XYZ coordinates at three-dimensional computer calculations of magnetic flux density, $\mathbf{B}_0(z)$, and initial magnetic flux, $\Phi_0(z)$.

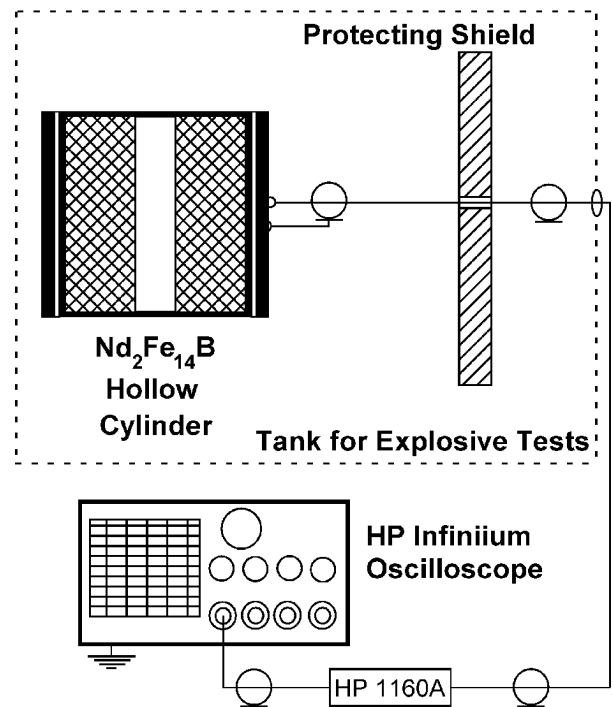


Fig. 14. The experimental setup for measuring the electromotive force, $E_g(t)$, generated due to the transverse shock wave demagnetization of the $\text{Nd}_2\text{Fe}_{14}\text{B}$ high-energy hard ferromagnetic hollow cylinder.

electromotive force normalized to the width of the coil

$$E_g(t) = \frac{1}{h} \int_0^h E_g(z, t) dz \quad (2)$$

where z is a coordinate along the axis of the hollow ferromagnetic cylinder (Fig. 13), $E_g(z, t)$ is the

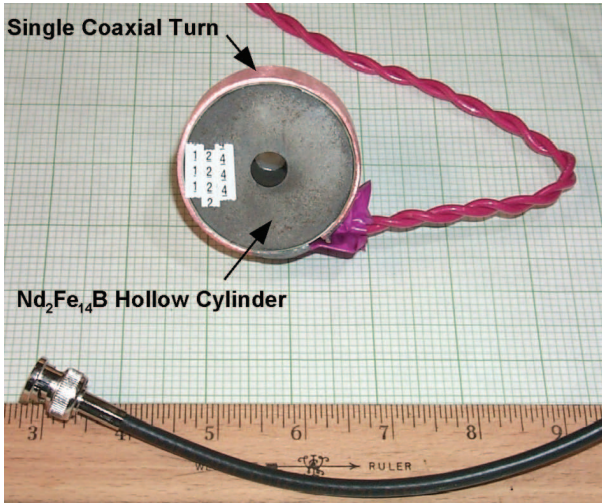


Fig. 15. The ultracompact FMG with the $\text{Nd}_2\text{Fe}_{14}\text{B}$ energy-carrying element ($O.D. = 5.08$ cm, $I.D. = 0.76$ cm, $h_0 = 1.27$ cm) prepared for charging explosive (C-4) and measuring electromotive force, $E_g(t)$, waveform.

momentary value of emf generated in single-turn coil with the width dz and placed in z coordinate.

In our devices, the h was always equal to the height of the $\text{Nd}_2\text{Fe}_{14}\text{B}$ hollow cylinder h_0 (Fig. 6). Therefore the $E_g(t)$ measured in the experiments is

$$E_g(t) = \frac{1}{h_0} \int_0^{h_0} E_g(z, t) dz. \quad (3)$$

The coil diameter in our devices was always 0.32 cm larger the diameter of the $\text{Nd}_2\text{Fe}_{14}\text{B}$ cylinder it was wound (Section 3.1). So, $E_g(t)$ measured in the experiments is the integral normalized electromotive force (Eq. 3) generated in the coil with diameter 0.32 cm larger the diameter of the ferromagnetic cylinder.

In accordance with the reason described above it is convenient to operate with the integral magnetic flux normalized to the width h_0 of the coaxial single-turn coil:

$$\Phi_{0in} = \frac{1}{h_0} \int_0^{h_0} \Phi_0(z) dz. \quad (4)$$

where $\Phi_0(z)$ is magnetic flux in cross-section of the coil wound. The Faraday's law can be written as follows

$$E_g(t) = \frac{1}{h_0} \int_0^{h_0} E_g(z, t) dz = -\frac{d}{dt} \frac{1}{h_0} \int_0^{h_0} \Phi_0(z) dz. \quad (5)$$

Since the magnetic flux $\Phi_0(z)$ in the center of the $\text{Nd}_2\text{Fe}_{14}\text{B}$ hollow cylinder is significantly higher than that at the cylinder butt-ends (see Figs. 18 and 19), decreasing the width of the coil wound on the

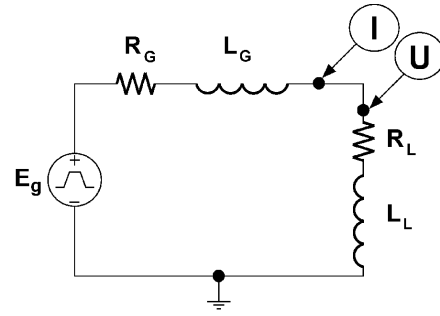


Fig. 16. The equivalent circuit employed for digital simulation of the seed current and the disposition of the probes measuring the seed current, $I(t)$, and the output voltage, $U(t)$, during the simulations ($IProbe$ and $UProbe$, respectively).

central part of the magnet leads to the increasing emf $E_g(t)$. This can be resulted in the increase of the generated current amplitude. At the same time, decreasing the width of the coil leads to increasing the coil resistance R_G and coil inductance L_G , which decrease the current amplitude and increase risetime (see Section 3.1). The analysis of this problem exceeds the limits of present work.

The integration of the $E_g(t)$ waveform from 0 to t

$$\Delta\Phi(t) = - \int_0^t E_g(t) dt \quad (6)$$

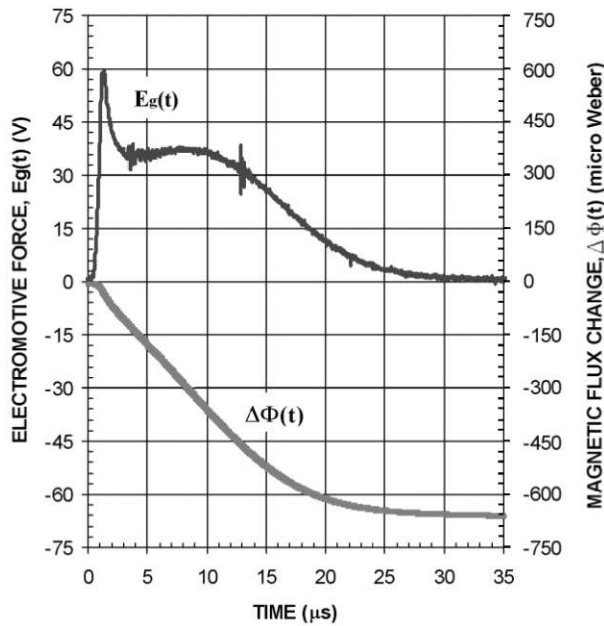
allows one to obtain the experimental value of the integral normalized magnetic flux change in the coaxial single turn coil due to the demagnetization of $\text{Nd}_2\text{Fe}_{14}\text{B}$ under the shock wave action at the moment of time t . The numerical value of the integral

$$\Delta\Phi_f = - \int_0^{+\infty} E_g(t) dt \quad (7)$$

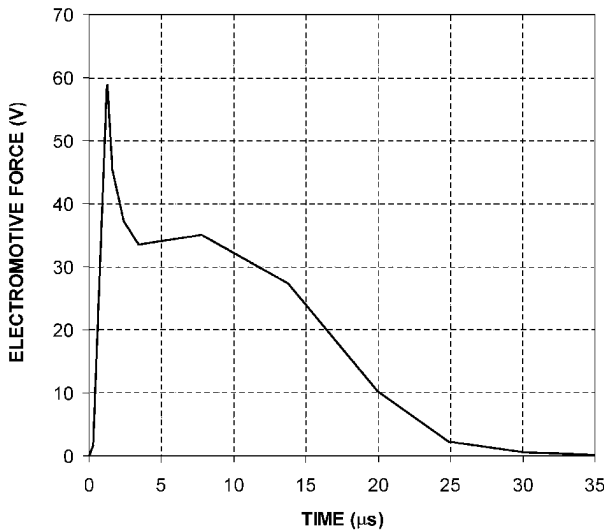
gives the experimental value of the total (final) decrease of the integral normalized magnetic flux in the coaxial single turn coil due to the demagnetization of $\text{Nd}_2\text{Fe}_{14}\text{B}$ under the shock wave action.

On the assumption that the magnetic flux carrier is demagnetized completely under the shock wave action, the experimentally obtained value of $\Delta\Phi_f$ Eq. (7) must be equal the value of the initial integral normalized magnetic flux, Φ_{0in} , Eq. (4) existing in the pulse-generating coil before shock wave action.

The accurate experimental measurement of the initial integral normalized magnetic flux Φ_{0in} (by measuring a function $\Phi_0(z)$ over the height of the $\text{Nd}_2\text{Fe}_{14}\text{B}$ hollow cylinder in the cross-section of pulse-generating coil having the diameter 0.32 cm larger then diameter of the ferromagnetic body) is extremely difficult-to-complete problem. Because of this, we employed the computer calculations of the



(a)



(b)

Fig. 17. (a) Typical waveform of the electromotive force, $E_g(t)$ (black), recorded from the coaxial single-turn coil wound on the $\text{Nd}_2\text{Fe}_{14}\text{B}$ hollow cylinder ($O.D. = 5.08$ cm, $I.D. = 0.76$ cm, $h_0 = 1.27$ cm), and the corresponding function of the integral normalized magnetic flux change in the coil $\delta\Phi = -\int_0^t E_g(t)dt$ (gray). (b) The $E_g(t)$ waveform digitized in the SOURCE section of the PSpice code.

initial magnetic flux density, $\mathbf{B}_0(z)$, initial magnetic flux, $\Phi_0(z)$, and the integral normalized magnetic flux, Φ_{0in} , using the ANSOFT Maxwell three-dimensional code. The schematic diagram illustrates the position of a coaxial single-turn coil containing $\text{Nd}_2\text{Fe}_{14}\text{B}$ hollow cylinder relatively XYZ coordinates at the computer

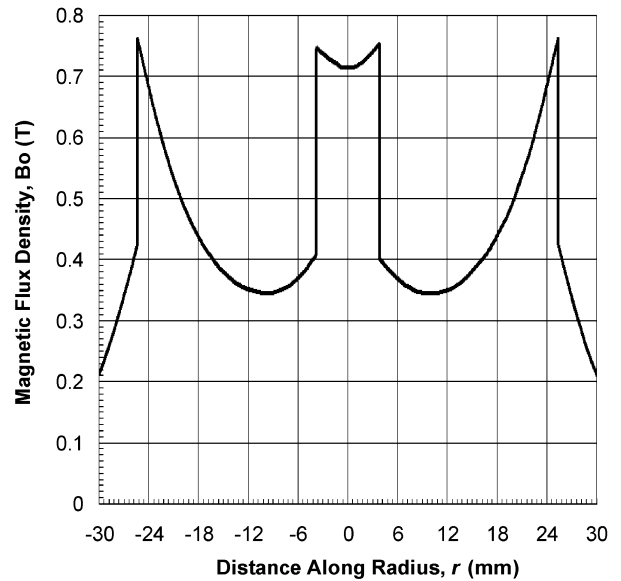


Fig. 18. Magnetic flux density, $\mathbf{B}_0(z = 0)$, inside and outside of the $\text{Nd}_2\text{Fe}_{14}\text{B}$ hollow cylinder having $O.D. = 5.08$ cm, $I.D. = 0.76$ cm, $h_0 = 1.27$ cm in the cut plane being offset in the middle of the cylinder.



Fig. 19. The initial magnetic flux, $\Phi_0(z)$, in the coaxial single-turn coil having diameter $D = 5.4$ cm wound on the $\text{Nd}_2\text{Fe}_{14}\text{B}$ hollow cylinder ($O.D. = 5.08$ cm, $I.D. = 0.76$ cm, $h_0 = 1.27$).

calculations performed is presented in Fig. 13. The beginning of XYZ coordinates is placed in the center of the coil.

The technique of the calculations contains two stages. First, the initial magnetic flux density, $\mathbf{B}_0(z)$, and initial magnetic flux, $\Phi_0(z)$, were computed in internal space of the pulse-generating coil that contains $\text{Nd}_2\text{Fe}_{14}\text{B}$ hollow cylinder. The second, the initial integral normalized magnetic flux in the pulse-generating coil Φ_{0in} was calculated using Eq. (4). The results of these calculations are presented in Figs. 18 and 19.

Series of special experiments were performed to obtain emf $E_g(t)$ waveforms that were needed to measure final decrease of the integral normalized magnetic flux $\Delta\Phi_f$ (Eq. 7) due to the demagnetization of $\text{Nd}_2\text{Fe}_{14}\text{B}$ under the shock wave action. In these experiments, the FMG with coaxial single-turn pulse-generating coil was loaded onto an Agilent 1160A miniature passive probe of input impedance 10 M Ω (Fig. 14). In this case, the current flowing in the circuit $I(t)$ is negligible ($I(t)_{\max} < 10^{-5}$ A) and the recorded waveform of the output voltage $U(t)$ can be put, with a good accuracy, identical to the waveform of the pulse of electromotive force $E_g(t)$. Figure 15 presents photograph of the FMG prepared for measuring $E_g(t)$

waveform. The results of the experiments performed are presented in Section 3.4.

As it follows from our investigations (see Section 3.4) the initial value of the magnetic flux Φ_{0in} existed in the pulse-generating coil before the shock action is practically equal to the experimentally obtained magnetic flux $\Delta\Phi_f$ lost under the shock wave action. Based on these results one can make the conclusion that developed in this work methodology of joint operating on the integral magnetic flux normalized to the width of the pulse-generating coil, Φ_{0in} , and the integral electromotive force waveform normalized to the width of the coil, $E_g(t)$, is correct. It gives the ground to consider the recorded in the experiments integral normalized electromotive force waveform, $E_g(t)$, as basic function which can be used in computer or analytical calculations for predicting the waveforms of voltage, $U(t)$, and current, $I(t)$, in any electric circuits powered by ultracompact explosive-driven current source based on transverse-shock-wave demagnetization of $\text{Nd}_2\text{Fe}_{14}\text{B}$ high-energy hard ferromagnets.

Since the goal of this work was a study of the generation of seed current produced by the generator loaded on the MCG seeding coil it was performed experimental investigations of pulsed power characteristics, in particularly, waveforms of output current, $I(t)$, and output voltage, $U(t)$, as well as computer calculations of these characteristics. The digital calculation technique is described in the next section.

3.3. Numerical Analysis of the Seed Current in the Circuit

Since the circuit parameters R_G , L_G , R_L , and L_L (Fig. 10b) can be measured directly, an efficient way to analyze the seed current $I(t)$ in the circuit is a digital simulation. For computer simulation of the output signals in the circuits we used commercial PSpice code [23].

The original basic cause of generating the seed current in the circuit is the electromotive force pulse $E_g(t)$ produced by the ultracompact generator. The $E_g(t)$ waveform recorded in the experiments with Agilent 1160A miniature passive probe served as a load of the coaxial single-turn pulse-generating coil of the FMG (Figs. 14 and 15) was digitized in the SOURCE section (VPWL source type) of the PSpice code after which the waveform of the seed current $I(t)$ was calculated. The equivalent circuit employed and the disposition of the probes measuring the output current $I(t)$ and the output voltage $U(t)$ during the simulations (*IProbe* and *UProbe*, respectively) are shown in Fig. 16.

3.4. Demagnetization of $\text{Nd}_2\text{Fe}_{14}\text{B}$ Energy-Carrying Elements Under the Transverse Shock Wave Action

$\text{Nd}_2\text{Fe}_{14}\text{B}$ energy-carrying elements of a transverse shock wave ultracompact FMG (Fig. 6) having outer diameter 5.08 cm, inner diameter 0.76 cm and length 1.27 cm (volume 25.1 cm³) were used in the experiments. The weight of the $\text{Nd}_2\text{Fe}_{14}\text{B}$ energy-carrying element is 185.7 g. For its operation, the generator calls for 0.6 g of an explosive (C-4).

The FMG prepared for charging explosive (C-4) and measuring $E_g(t)$ waveform is shown in Fig. 15. The waveform of typical emf pulse $E_g(t)$ produced by the ultracompact FMG loaded onto Agilent 1160A probe and the corresponding function of the integral normalized magnetic flux change in the coaxial single-turn coil due to the demagnetization of $\text{Nd}_2\text{Fe}_{14}\text{B}$ under the shock wave action $\Delta\Phi(t) = -\int_0^t E_g(t)dt$ are given in Fig. 17(a).

The peak value of the induced $E_g(t)$ is 59.2 V. The FWHM is 12.3 μs . The waveform has an extended right edge of length more than 35 μs . The experimentally obtained waveform of $E_g(t)$ was digitized in the SOURCE section (VPWL type source) of the PSpice code. Digitized emf pulse, $E_g(t)$, is shown in Fig. 17(b).

The experimental value of the final decrease of the integral normalized magnetic flux $\Delta\Phi_f$ due to the shock wave demagnetization of the $\text{Nd}_2\text{Fe}_{14}\text{B}$ energy-carrying element is

$$\Delta\Phi_f = -\int_0^{+\infty} E_g(t)dt = 733 \pm 27 \mu\text{Wb}.$$

The computed initial magnetic flux density \mathbf{B}_0 inside and outside of the $\text{Nd}_2\text{Fe}_{14}\text{B}$ cylinder for the plane being offset in the middle of the cylinder and $\Phi_0(z)$ function of initial magnetic flux in cross-section of the pulse-generating coil are presented in Fig. 18 and Fig. 19, correspondingly. The computed initial integral normalized magnetic flux in the coil is

$$\Phi_{0in} = \frac{1}{h_0} \int_0^{h_0} \Phi_0 dz = 754.5 \mu\text{Wb}.$$

The experimentally obtained magnetic flux loss $\Delta\Phi_f$ is almost equal to the initial value of the magnetic flux Φ_{0in} . The spread in the experimental values of the magnetic flux loss $\Delta\Phi_f$ does not exceed the industry tolerance of the principal magnetic parameters of the $\text{Nd}_2\text{Fe}_{14}\text{B}$ cylinders used in experiments. It is direct evidence that the $\text{Nd}_2\text{Fe}_{14}\text{B}$ hollow cylinders are demagnetized almost completely

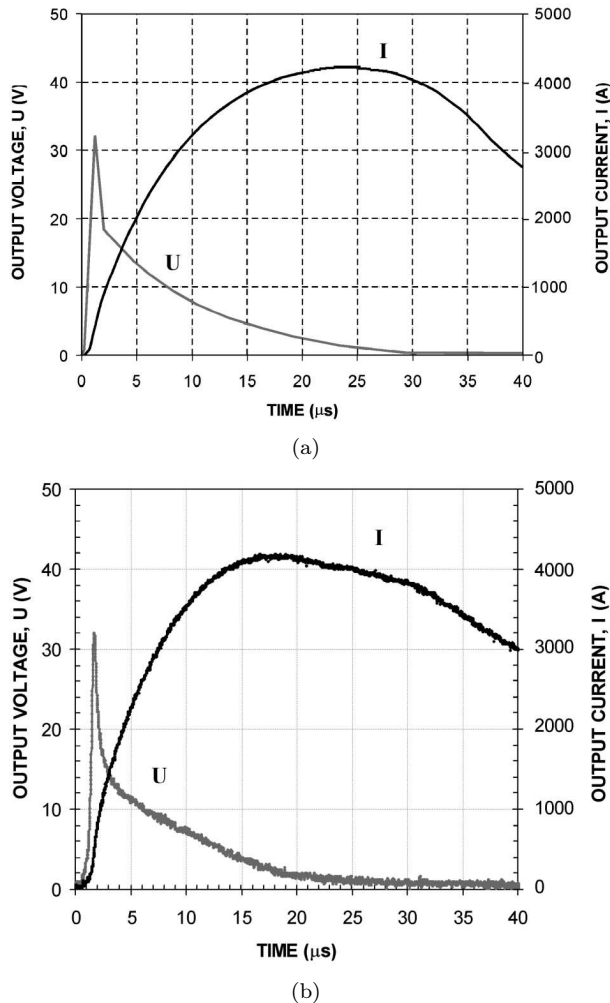


Fig. 20. (a) The results of the computer calculations of the FMG output current, $I(t)$ (black), and output voltage, $U(t)$ (gray), for the first 35 μs after initiation of the shock wave in the $\text{Nd}_2\text{Fe}_{14}\text{B}$ energy-carrying element ($O.D. = 5.08$ cm, $I.D. = 0.76$ cm, $h_0 = 1.27$). (b) The experimental waveforms of the FMG output current, $I(t)$ (black), and voltage, $U(t)$ (gray), recorded for the same period of time. The impedance of the load $Z_L(100$ kHz) $= 18$ m Ω .

by 0.6 g of explosive (C-4).

In this reason all electromagnetic energy stored in this energy-carrying element is released and can be transformed in the pulse of high current. The high current pulse can be the sought-for seed current of a MCG. The results of investigations of transducing electromagnetic energy stored in $\text{Nd}_2\text{Fe}_{14}\text{B}$ in the seed current are given.

3.5. Current Produced by the Ultracompact Ferromagnetic Primary Source

The general design of the system including MCG seeding coil served as a load of the FMG is shown in

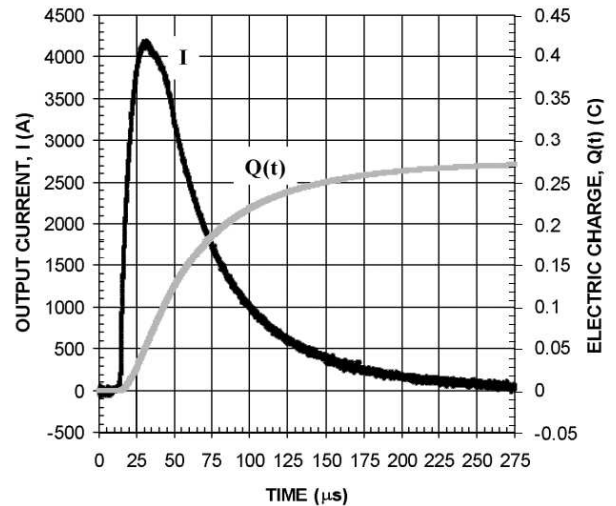


Fig. 21. The experimental full-scale waveform of the FMG output current, $I(t)$ (black), and evolution of the charge passed through the circuit, $Q(t) = \int_0^t I(t)dt$ (gray). The impedance of the load $Z_L(100$ kHz) $= 18$ m Ω .

Fig. 11. Experiments were performed with a load made as an MCG coaxial single-turn seeding coil. The coil was made of copper strip (thickness 0.1 cm). The coil was made so that its electric parameters represented the parameters of the typical coaxial single-turn seeding coil of a mini MCG [1–3]. The coil had absolute value of impedance $Z_L(100$ kHz) $= 18$ m Ω , inductance $L_L(100$ kHz) $= 29$ nH, equivalent serial resistance $R_S(100$ kHz) $= 2.7$ m Ω . The schematic diagram of the experimental system for measuring seed current is shown in Fig. 9.

To make correct experimental setup for seed current measurement we performed a computer calculations of $I(t)$ and $U(t)$ in the circuit using technique described in Sections 3.2 and 3.3. Experimentally obtained waveform of $E_g(t)$ (that was digitized in the SOURCE section of the PSpice code Fig. 17) was used in the calculations.

Figure 20a presents the results of PSpice calculations of the seed current $I(t)$ and the output voltage $U(t)$ for first 35 μs after ignition of the shock wave in the $\text{Nd}_2\text{Fe}_{14}\text{B}$. Electrical parameters of the generator were as following: $R_G(100$ kHz) $= 5.2$ m Ω , $L_G(100$ kHz) $= 38$ nH.

The calculated peak amplitude of the current is $I(t)_{\text{max}} = 4200$ A. The risetime of the current $I(t)$ from zero to its maximum value $I(t)_{\text{max}} = 4200$ A is 21 μs . The calculated peak amplitude of the output voltage pulse is $U(t)_{\text{max}} = 30$ V with an $FWHM = 2.6$ μs .

The FMG before and after high-current test is shown in Fig. 12. The experimental waveforms of the FMG output current $I(t)$ and output voltage

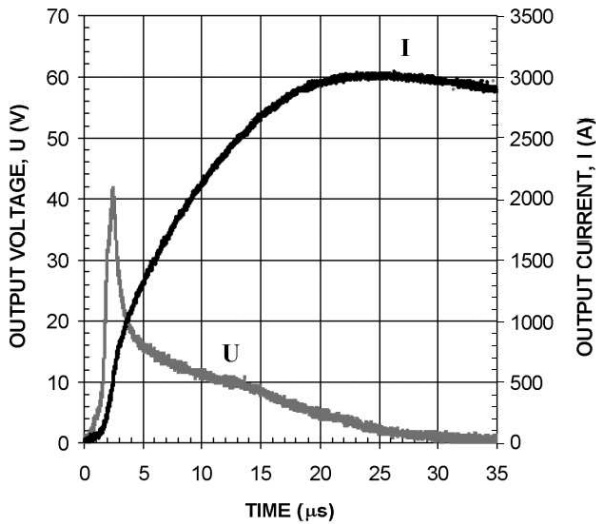


Fig. 22. Experimental waveforms of the seed current, $I(t)$ (black), and voltage, $U(t)$ (gray), produced by the ultracompact FMG in the coaxial single-turn seeding coil of mini-MCG during first 35 μs after initiation of the shock wave in the $\text{Nd}_2\text{Fe}_{14}\text{B}$ energy-carrying element.

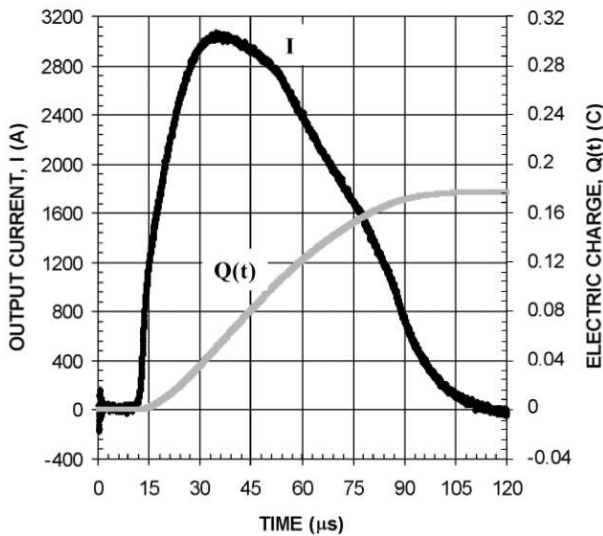


Fig. 23. The experimental full-scale waveform of the MCG seed current, $I(t)$ (black), and the evolution of the charge passed through the circuit $Q(t) = \int_0^t I(t)dt$ (gray).

$U(t)$ are presented in Fig. 20b. Comparing Figs. 20a and 20b one can make a conclusion about good coincidence of experimental and calculated waveforms. Thus, the measured seed current maximum and the output voltage peak, respectively $I(t)_{\text{max}} = 4180 \text{ A}$ and $U(t)_{\text{max}} = 31.8 \text{ V}$. The measured time of rise of the seed current $I(t)$ from zero to its peak value $I(t)_{\text{max}} = 4180 \text{ A}$ is $18.2 \mu\text{s}$. The FWHM for the recorded waveform of the output voltage $U(t)$ is $1.5 \mu\text{s}$.

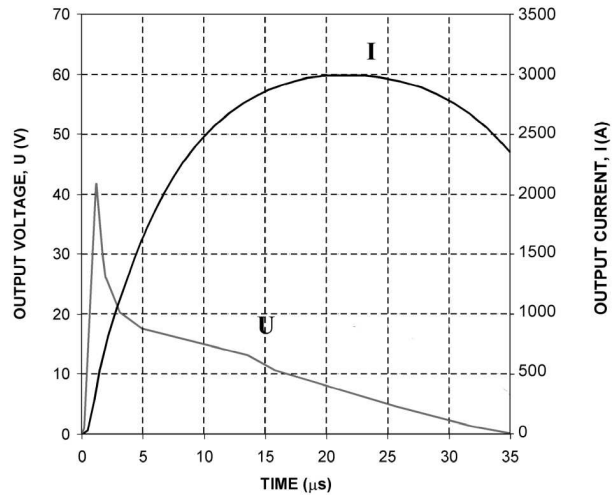


Fig. 24. Computer simulated waveforms of the MCG seed current, $I(t)$ (black), and voltage, $U(t)$ (gray), for the first 35 μs after initiation of the shock wave in the $\text{Nd}_2\text{Fe}_{14}\text{B}$ energy-carrying element of the ferromagnetic primary source.

The recorded full-scale waveform of the seed current $I(t)$ represents a quasi-triangular pulse with $50 \mu\text{s}$ FWHM (Fig. 21).

Figure 19 also shows the evolution of the charge passed through the circuit:

$$Q(t) = \int_0^t I(t)dt. \quad (8)$$

The total charge passed through the circuit during the experiment is

$$Q(\infty) = \int_0^{+\infty} I(t)dt = 0.27 \text{ C},$$

which is greater by three or four orders of magnitude than the integrated charge transferred by a current source of primary energy based on shock wave depolarization of piezoceramics [20].

3.6. Seeding of Spiral Mini-MCG by Explosive-Driven Ferromagnetic Primary Source

To illustrate further the operation of an ultracompact FMG as a seed source of an MCG the design of an autonomous completely explosive pulsed power system with two coaxial coils has been explored (Fig. 8). The coaxial single-turn pulse-generating coil of the FMG having $\text{Nd}_2\text{Fe}_{14}\text{B}$ energy-carrying element was connected by the strip transmission line with the coaxial single-turn MCG seeding coil ($D = 4.5 \text{ cm}$). The MCG helix containing 57 turns of copper wire was wound inside of the

MCG single-turn seeding coil. The outer diameter of the MCG aluminum liner loaded with C-4 high explosive was 9.5 mm. Liner inner diameter was 7.6 mm. Completely explosive pulsed power system contained three RP-501 detonators: two detonators of the ferromagnetic primary source and one detonator of the MCG liner. All three detonators were ignited at the same moment of time.

The seed coil of the MCG had absolute value of impedance $Z_L(100\text{kHz})= 41 \text{ m}\Omega$, inductance $L_L(100 \text{ kHz})= 62 \text{ nH}$, equivalent serial resistance $R_S(100 \text{ kHz})= 6.1 \text{ m}\Omega$. The $\text{Nd}_2\text{Fe}_{14}\text{B}$ energy-carrying element of the FMG had outer diameter 5.08 cm, inner diameter 0.76 cm and length 1.27 cm. The mass of C-4 charge loaded in the FMG was 0.62 g. The mass of C-4 charge loaded in the MCG liner was 13.4 g.

Waveforms of the seed current $I(t)$ and output voltage $U(t)$ produced by the FMG in the seeding coil of the mini-MCG for the first 35 μs after ignition of the shock wave in the $\text{Nd}_2\text{Fe}_{14}\text{B}$ is shown in Fig. 22. The maximum of the seed current is $I(t)_{\text{max}} = 3030 \text{ A}$. The time of rise of the seed current $I(t)$ from zero to its peak value $I(t)_{\text{max}} = 3030 \text{ A}$ is 24.1 μs .

The full-scale waveform of the seed current $I(t)$ and the evolution of the total charge passed through the circuit during the experiment are shown in Fig. 23. The FWHM of the quasi-triangle current pulse is 64 μs .

The total charge is $Q(\infty) = \int_0^{+\infty} I(t)dt = 0.177 \text{ C}$.

The results of the test performed allow make the conclusion that real explosive-driven MCG can be successfully seeded by the developed in this work ultracompact FMG. We have shown conceptual possibility of powering an MCG by an FMG. The traditional seeding system containing a capacitor bank, charging circuit, a primary energy storage (batteries) and a switch was replaced by really small explosive-driven high-current primary source. This completely explosive autonomous pulsed power system is smaller, lighter and more reliable in operation than traditional MCG powered by a capacitor bank.

We performed computer simulation of the process of seeding the MCG in the completely explosive pulsed power system. Figure 24 presents the results of calculations of the seed current $I(t)$ and the output voltage $U(t)$ for first 35 μs after ignition of the shock wave in the $\text{Nd}_2\text{Fe}_{14}\text{B}$. Electrical parameters of the generator were as following: $R_G(100 \text{ kHz})= 5.2 \text{ m}\Omega$, $L_G(100 \text{ kHz})= 38 \text{ nH}$.

The calculated peak amplitude of the current is $I(t)_{\text{max}} = 2970 \text{ A}$. The calculated risetime of the current $I(t)$ from zero to its maximum value is 20 μs . The calculated peak amplitude of the output voltage pulse is $U(t)_{\text{max}} = 40.2 \text{ V}$ with an $FWHM = 2.3 \mu\text{s}$.

Comparison of the seed current waveform experimentally recorded and computer calculated

(Figs. 22 and 24) shows a good agreement peak amplitude and risetime of actual and digitally simulated signals. It allows one to make the conclusion that developed methodology of digital simulation of the operation of the ferromagnetic primary source can be successfully used for prediction seed current parameters in the combined FMG/MCG completely explosive pulsed power systems.

4. Summary

Experimental investigations and digital simulations of the generation of seed currents by an ultracompact generator based on transverse shock wave demagnetization of $\text{Nd}_2\text{Fe}_{14}\text{B}$ high-energy hard ferromagnets, loaded onto a coaxial single-turn seeding coils of a magnetocumulative generator were conducted. The seed current produced by the transverse shock wave ferromagnetic generators with relatively small dimensions of the $\text{Nd}_2\text{Fe}_{14}\text{B}$ energy-carrying elements (25 cm^3 in volume) reaches 4.18 kA in amplitude and FWHM of 50 μs .

Developed methodology of digital simulation of the seeding processes in the combined FMG/MCG system provides correct prediction of the output parameters in the electric circuit. This method can be also used to predict output parameters in other electric circuits powered by ultracompact explosive-driven current source based on transverse-shock-wave demagnetization of $\text{Nd}_2\text{Fe}_{14}\text{B}$ high-energy hard ferromagnets.

The results obtained allow make the conclusion that the ultracompact FMG can be considered as most reliable and matched source of primary power for a magnetocumulative generator.

Acknowledgement

Authors thank Professor Magne Kristiansen (Texas Tech University) and Dr. Larry L. Altgilbers (U.S. Army Space and Missile Defense Command) for their attention and support of this work.

Manuscript received October 28, 2003

References

- [1] Megagauss Magnetic Field Generation and Pulsed Power Application edited by M. Cowan and R.B. Spielman – New York: Nova Science Publ. – 1994.
- [2] Megagauss and Megaampere Pulse Technology and Applications, edited by V.K. Chernyshev, V.D. Selemir, and L.N. Plyashkevich – Russia, Sarov: VNIIEF Press. – 1997.

- [3] Altgilbers L.L., Brown M.D.J., Grishnaev I., Novac B.M., Smith I.R., Tkach I., Tkach Yu. Magnetocumulative Generators – New York: Springer-Verlag. – 2000.
- [4] Neilson F.W. and Anderson G.W. // Bulletin of American Physical Society. – 1957. – V. 2. – P. 302.
- [5] Kulterman R.W., Neilson F.W. and Benedick W.B. // Journal of Applied Physics. – 1958. – V. 29. – P. 500–503.
- [6] Graham R.A. // Journal of Applied Physics. – 1968. – V. 39. – P. 437–524.
- [7] Wayne R.C. // Journal of Applied Physics. – 1969. – V. 40. – P. 15–21.
- [8] Keeler R.N. and Royce E.B. // in Proceedings of the International School of Physics "Enrico Fermi", Villa Monastero, Italy, 4-26 July, 1969, Course XLVIII, edited P. Caldirola and H. Knoepfel (Academic Press, NY, 1971) – P. 51–150.
- [9] Campbell P. Permanent Magnet Materials and Their Application – Cambridge: Cambridge University Press. – 1994.
- [10] Shkuratov S.I., Talantsev E.F., Dickens J.C. and Kristiansen M. // Journal of Applied Physics. – 2002. – V. 91. – P. 3007–3009.
- [11] Shkuratov S.I., Talantsev E.F., Dickens J.C. and Kristiansen M. // Applied Physics Letters. – 2003. – V. 82. – P. 1248–1250.
- [12] Shkuratov S.I., Talantsev E.F., Dickens J.C. and Kristiansen M. // IEEE Transactions on Plasma Science. – 2002. – V 30, No. 5. – P. 1681–1691.
- [13] Shkuratov S.I., Talantsev E.F., Dickens J.C., and Kristiansen M. // Journal of Applied Physics. – 2002. – V. 92. – P. 159–162.
- [14] Shkuratov S.I., Talantsev E.F., Dickens J.C., and Kristiansen M. // Review of Scientific Instruments. – 2002. – V. 73. – P. 2738–2742.
- [15] Shkuratov S.I., Talantsev E.F., Dickens J.C., and Kristiansen M. // Journal of Applied Physics. – 2003. – V. 93. – P. 4529–4535.
- [16] Bozorth R.M. Ferromagnetism – NJ: IEEE Press, Piscataway. – 1993.
- [17] Talantsev E.F., Shkuratov S.I., Dickens J.C. and Kristiansen M. // Modern Physics Letters B. – 2002. – V. 16, N 15& 16. – P. 545–554.
- [18] High-Power Microwave Sources and Technologies, edited by Barker R.J. and Shamiloglu Edl – NY: IEEE Press. – 2001.
- [19] Talantsev E.F., Shkuratov S.I., Dickens J.C., and Kristiansen M. // Review of Scientific Instruments. – 2003. – V. 74, No. 1, Part I. – P. 225–230.
- [20] Shkuratov S.I., Talantsev E.F., Dickens J.C., Kristiansen M., Altgilbers L.L., Tkach Y., and Tracy P.T. // IEEE Transactions on Plasma Science. – 2002. – V. 30, No. 5. – P. 1665–1673.
- [21] Ansoft Corporation, Four Station Square, Suite 660, Pittsburgh PA 15219, www.ansoft.com
- [22] Johnson J.H. // Journal of Applied Physics. – 1959. – V. 30. – P. 241S–242S.
- [23] Cadence PCB Design Solutions, www.cadencepcb.com. OrCad PCB, www.orcadpcb.com. Pspice PCB, www.pspicepcb.com.